Journal of Membrane Science 659 (2022) 120791

Contents lists available at ScienceDirect

Journal of Membrane Science

journal homepage: www.elsevier.com/locate/memsci

Visualizing protein fouling and its impact on parvovirus retention within distinct filter membrane morphologies

Remo Leisi [a,b,*], Iman Rostami [a], Andrew Laughhunn [c], Jan Bieri [a], Nathan J. Roth [b], Eleonora Widmer [b], Carlos Ros [a]

[a] Department of Chemistry, Biochemistry, and Pharmaceutical Sciences, University of Bern, Freiestrasse 3, 3012, Bern, Switzerland
[b] CSL Behring AG, Wankdorfstrasse 10, 3000, Bern 22, Switzerland
[c] CSL Behring, 1st Ave 1020, 19406, King of Prussia, PA, USA

ARTICLE INFO

Keywords:
Virus filtration
Filter fouling
Parvovirus retention
Flow decay
Membrane structure

ABSTRACT

Virus filtration is considered an effective and robust method to remove viral contaminants that may enter the manufacturing process of biotherapeutics. However, insights into the retention mechanism of viruses under the influence of different operating conditions have been limited so far. In this work, we visualize the impact of filter fouling and flow decay on the retention of fluorescently labeled minute virus of mice (MVM) in asymmetric Planova 20N and nearly homogeneous Pegasus SV4 filter membranes. Filtration of feedstreams containing polyclonal human immunoglobulin G (IgG) revealed a complex interplay of different fouling mechanisms depending on high- or low-fouling solution properties, and characteristic for the distinct filter types. The asymmetric filter morphology – which allowed gradual foulant deposition across membrane zones with different pore sizes – provided a larger capacity for capture of fouling particulates as well as robust virus retention under challenging feedstream conditions. Taken together, our results demonstrate that different filtration conditions can lead to a combination of various, even opposing effects on virus retention depending on the membrane structure and pore size characteristics. The phenomena visualized in this work contribute to a better understanding of the underlying molecular mechanisms and provide cues for specific optimization of virus filtration processes.

1. Introduction

Therapeutic products derived from biological sources carry the inherent risk of viral contaminations. Mammalian cell cultures used to produce recombinant biotherapeutics are known to endogenously express retrovirus-like particles, as well as their susceptibility to infections by adventitious viruses [1,2]. Plasma donations, which serve as raw material for the manufacturing of plasma-derived medicinal products, such as polyclonal human immunoglobulin G (IgG), potentially contain blood-borne viruses. To assure virus safety, manufacturers employ a multi-layered strategy to mitigate the risk of viral contaminations by rigorous monitoring of sources and testing of raw materials, while incorporating effective virus clearance steps to eliminate potentially present viruses during the downstream processing [3].

Virus filtration (VF) is considered one of the most effective and robust methods to remove any viral contaminant potentially introduced into the manufacturing process based on a size-exclusion mechanism. The small and highly stable parvoviruses, such as minute virus of mice (MVM), represent a relevant contamination risk for biologicals and are generally accepted as a worst-case model to validate the effectiveness of virus clearance steps [4,5]. Parvovirus-grade filters composed of polymeric membranes with nominal pore sizes in the range of 19–20 nm provide selective separation between therapeutic proteins, such as IgGs with a hydrodynamic diameter of 10–12 nm, and parvoviruses with an outer capsid diameter of 27–29 nm [6–9].

The macromolecules present in the downstream manufacturing of biotherapeutics have the potential to self-associate, aggregate or interact with surfaces, such as polymeric filter materials, causing membrane

Abbreviations: DOL, degree of labeling; Immunoglobulin G, IgG; LSM, laser scanning microscopy; LRF, log10 reduction factor; MVM, minute virus of mice; NHS-Atto, N-hydroxy-succinimide ester-modified Atto dye; PBS, phosphate buffered saline; PVDF, poly(vinylidene fluoride); qPCR, quantitative polymerase chain reaction; SDS-PAGE, sodium dodecyl sulfate polyacrylamide gel electrophoresis; VF, virus filtration; VRP, virus retention profile.

* Corresponding author. CSL Behring AG, Wankdorfstrasse 10, 3000, Bern 22, Switzerland.
E-mail address: remo.leisi@cslbehring.com (R. Leisi).

https://doi.org/10.1016/j.memsci.2022.120791
Received 29 April 2022; Received in revised form 24 June 2022; Accepted 1 July 2022
Available online 5 July 2022

fouling. In VF, fouling of the membrane is a critical challenge that can significantly limit the filter performance by reducing the product throughput and compromising the effectiveness of virus removal [10–12].

Different fouling mechanisms have previously been described by Hermia et al. [13,14]: Standard blocking, also known as pore constriction, which is a consequence of deposition/adsorption of proteins at the walls of the pores; complete (pore) blockage, where the pores are plugged through aggregates with a size similar or slightly larger than the pore diameter; intermediate blocking, where pores are only partially blocked by the fouling particles; cake filtration, where a permeable layer of foulants is formed on the membrane by continuous deposition of bulk protein. Mathematical modeling was used to describe the different fouling effects during filtration, illustrating that membrane fouling is a result of combined mechanisms, which dynamically change during the progression of filtration [15–19]. Flow decay in protein filtration is generally understood as a consequence of primarily irreversible fouling involving protein aggregates in the size range of the filter pores, that are formed before or during filtration [11,20–23]. Trace quantities of protein species in the feedstream having the propensity to self-associate serve as nucleation sites for continued deposition of bulk protein in the sieving layer of the membrane [18,24–26]. In line with this, the throughput of IgG feedstreams in VF could be considerably improved by using prefilters that remove hydrophobic, self-associating protein species, such as oxidized or degraded IgG forms [22,27–31].

Intra- or intermolecular interactions between proteins in the feedstream and the membrane are dependent on their isoelectric point (pI), the solution pH, and conductivity. Consequently, fouling is critically impacted by specific filtration conditions, the therapeutic protein, and filter membrane material [11,19,21,25,32–35]. Therefore, careful evaluation and control of these factors are essential to reduce membrane fouling and maximize product throughput.

Furthermore, filter fouling can substantially affect the effectiveness of virus removal by i) the occupation of retentive pores through virus-sized fouling aggregates, which redirects the flow to non-retentive pathways [10,36,37]; ii) flow decay, which allows for increased lateral diffusion of viruses to access non-retentive pores [12,37–39]; iii) pore constriction, which leads to pore size reduction and earlier retention of viral particles in the filter [40,41]. In addition to these size-based, physical effects, adsorptive interactions should also be considered, such as virus-virus, virus-protein, and virus-membrane interactions, which again depend on the specific physico-chemical properties of the involved components [23,37,39,42].

In summary, VF is a highly complex process involving multiple factors, with performance influenced by inadequately understood mechanisms. The stepwise dissection of the different contributing factors is often approached to simplify the investigated system, e.g., by using standard proteins, standard conditions, and non-infectious surrogates instead of relevant virus models. Numerous studies have investigated the membrane fouling mechanisms including mathematical modeling in the context of micro- and ultrafiltration processes, assuming single-layer membranes with cylindrical, uniform, and straight pores [15–18]. The composition of most virus filter membranes, with their intricate, interconnected pore structure, characteristic pore size gradients, and variable pore size distributions, enable different fouling mechanisms to occur simultaneously in multiple layers [10,19]. Advanced analytical approaches have been used to visualize the fouling entities and virus-sized particles directly inside the distinct membrane morphologies to confirm proposed mechanisms and to further resolve the interplay of the different factors [18,26,40,41,43,44].

The objective of this work was to generate a deeper understanding of filter fouling by comparing distinct membrane types and varying conditions in the relevant context of parvovirus filtration. To this end, we labeled IgG and MVM with fluorescent dyes and simultaneously visualized their retention in Planova 20N and Pegasus SV4 filters by using laser scanning microscopy (LSM). Primarily, we generated mechanistic insights into the effects of low- and high-fouling polyclonal IgG feedstreams under "standard" conditions in PBS, pH 7.4, and finally compared these results to typical manufacturing conditions for a highly pure IgG product intermediate.

2. Materials and methods

2.1. Cells and viruses

The minute virus of mice prototype (MVMp) clone commonly used in validation studies performed in biopharmaceutical industry settings was obtained from ATCC (USA) [45]. Mouse A9 fibroblasts derived from ATCC were cultured in Dulbecco's modified Eagle's medium (DMEM), 5% fetal calf serum (FCS) at 37 °C, 5% CO_2.

2.2. Purification and characterization of MVM

Propagation, purification, and characterization of MVM were performed as previously described [46,47]. Briefly, mouse A9 fibroblasts cells were inoculated with MVM and harvested 3 days post-infection. Cells were washed with phosphate-buffered saline (PBS) and then lysed in PBS by three freeze-thaw cycles. The lysate was clarified by low-speed centrifugation and incubated with 0.1% Nonidet-P40 (NP-40) for 1 h at 4 °C. Clarified and sterile filtered cell lysate was layered on 20% sucrose and viruses were pelleted by ultracentrifugation at 150000×*g*. The pellet was resuspended in a small volume of the bottom fraction and analyzed for yield and purity. Purity and quantity of viral particles were determined by densitometric analysis of Coomassie-stained sodium dodecyl sulfate polyacrylamide gel electrophoresis (SDS-PAGE).

2.3. Labeling of MVM and IgGs with amine-reactive Atto dyes

Labeling of purified MVM and human polyclonal IgGs (Merck, G4386, purity ≥99%, Germany) with fluorescent dyes was performed similar to previously described [41,47]. Briefly, viruses or IgGs were incubated with amine-reactive N-hydroxy-succinimide ester-modified Atto dyes (NHS-Atto; Atto-Tec, Germany) to achieve crosslinking to surface lysines. After quenching the reaction, Atto-633 labeled virions were purified by ultracentrifugation through a 20% sucrose cushion. Atto-488 labeled IgGs were purified by size-exclusion chromatography using PD-10 columns (GE Healthcare, USA). The degree of labeling (DOL) was analyzed based on A_{280} to maximal absorption (A_{max}) of the fluorescent dye. Labeling was performed to obtain a limited DOL of about 25 dyes per viral capsid and 1 dye per IgG molecule, respectively, to achieve a reasonable compromise between sufficient signal and negligible impact on retention [46,47].

2.4. Nanofiltration of Atto-labeled viruses in different filter types

VF experiments were performed with Planova 20N (Asahi Kasei, Japan) and Pegasus SV4 (Pall Corporation, USA) filters, using commercially available small-scale membranes derived from the same production lot. Unless indicated, VF was carried out under standard operating conditions at room temperature (21–25 °C) and constant pressure following the manufacturer's instructions (Planova 20N, 0.8–0.9 bar; Pegasus SV4, 2.0–2.1 bar). Feedstreams for VFs consisted as indicated of PBS, pH 7.4; 1 mg/mL polyclonal human IgGs (Merck, G4386) in PBS; 10 mg/mL IgGs in PBS; or polyclonal human IgG product intermediate (10–14 mg/mL IgG, sodium acetate/phosphate buffer, pH 4.8, 0.5 mS/cm). A feedstream volume of 50 mL was spiked with 1 μg of viral capsids, corresponding to 1.5×10^{11} MVM particles, and passed through a 0.1 μm poly(vinylidene fluoride) (PVDF) filter (Merck Millipore). According to previous studies using similar spiking doses, no overspiking effects such as decrease of virus removal performance or flow decay during the small-scale filtration (0.001 m^2) were observed

[46–49]. Comparable spiking doses with purified unlabeled MVM corresponded to a total viral load of ~6.7 log10 TCID50 as measured on A9 cell culture. For analysis of viral load reduction, a feed sample and several filtrate fractions were collected. For visualization of IgG retention, Atto-488 labeled IgG was spiked into the feed corresponding to 1:100 of the used IgG concentration. Filter flow (J) was measured based on time to reach fraction volume and shown as relative filtrate flow (J/J0) in comparison to H20 flux (J0).

2.5. Analysis of filter membranes by laser scanning microscopy (LSM)

Virus filter membranes were prepared and analyzed as previously described [47]. Briefly, membranes were embedded in 2% low EEO agarose (PBS), cross-sectioned and analyzed using the laser scanning microscope 880 with a 63 × magnification objective (Carl Zeiss, Germany). To visualize filter dimensions and structure, the membrane autofluorescence was detected at λ_{ex} 405 nm; λ_{em} 422 nm. For 3D analysis of the intact membrane segments, scanning was performed with 20 × magnification objectives and autofluorescence at λ_{ex} 425 nm. Acquired data was processed with the ZEN program (Carl Zeiss) and exported as TIFF files. Images were analyzed with the ImageJ program [50] and data was processed with GraphPad Prism to obtain retention profiles as a function of the filter depth. Importantly, minor differences in membrane thickness due to cutting direction did not change relative filter depth of retained molecules; fouling and virus retention patterns were homogeneous and consistent across different membrane sections (Fig. 1A) (Supplementary Figs. 1–3).

2.6. Quantification of parvovirus reduction by qPCR

The concentration of MVM virions in the feed and filtrate fractions was determined by an optimized quantitative polymerase chain reaction (qPCR) protocol incorporating a nuclease treatment before DNA extraction as previously described [46,51]. Viral DNA was extracted (DNeasy Blood and Tissue Kit; Qiagen) and quantified by qPCR using MVM-specific primers, and an infectious clone of MVM as an external standard. Amplification and real-time detection were carried out with the CFX96 Real-Time system (Bio-Rad, USA). Log10 reduction factors (LRFs) were calculated based on different starting quantity of virions detected in the extracted feed and filtrate samples.

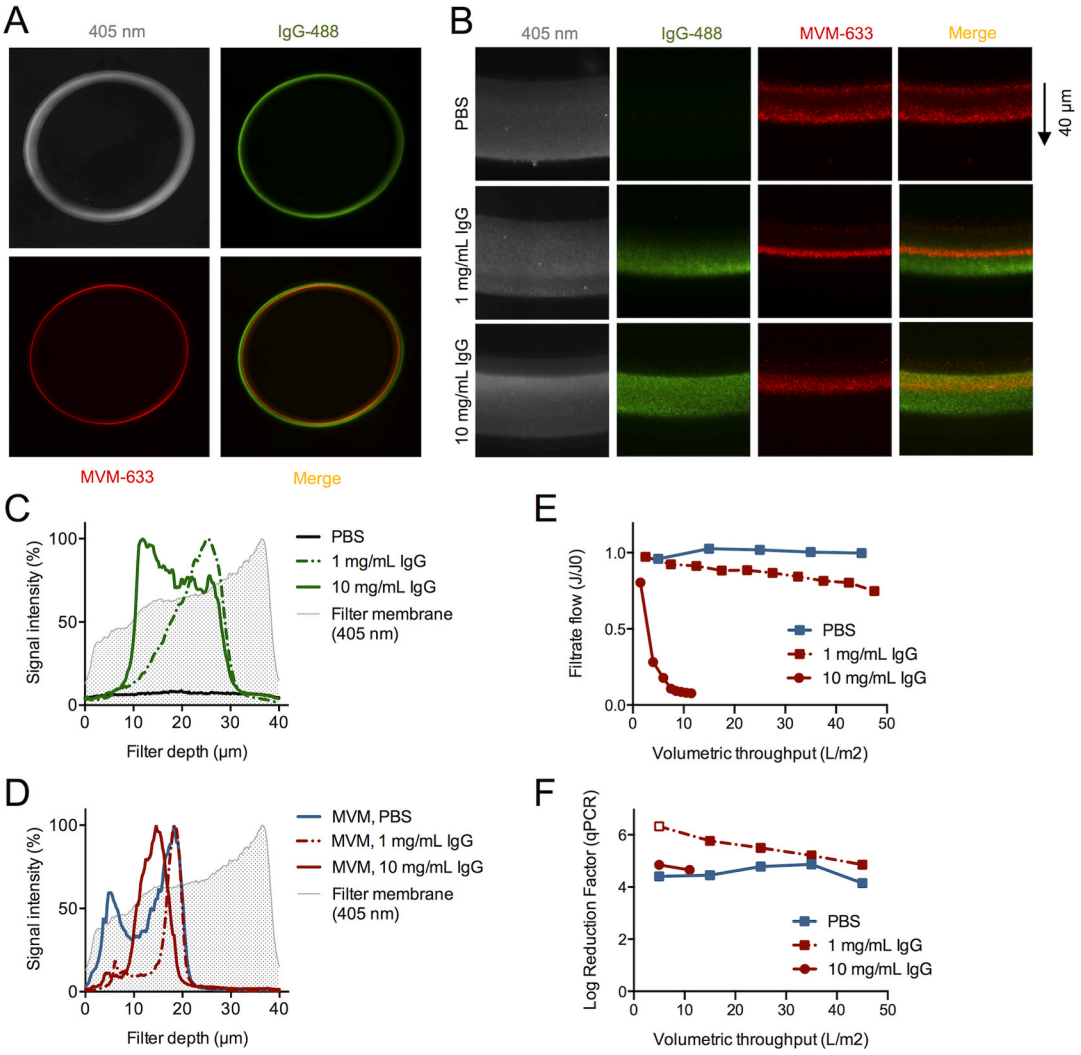

Fig. 1. Filter fouling and parvovirus retention in Planova 20N membrane. A) Laser-scanning microscopy images of a Planova 20N hollow fiber cross-section after filtration of 1 mg/mL IgG spiked with a minor proportion of Atto-488 labeled IgG (1:100) and Atto-633 labeled MVM (20x objective). B) Magnification into membrane segments (63x objective) after filtration of MVM-spiked PBS, 1 mg/mL IgG in PBS, or 10 mg/mL IgG in PBS. Retention profiles of C) IgG foulants and D) MVM-633 based on ImageJ analysis [50]. E) Relative filter flow (J/J0) of different feedstreams. F) Log10 reduction factors (LRFs) determined by qPCR of virions in feed and filtrate samples. Graphs show one filtration per condition (n = 1).

3. Results and discussion

To generate visual insights into the fouling mechanisms and its impact on virus retention inside the filter membrane by LSM, viruses and the therapeutic protein were labeled with fluorescent dyes prior to the filtration process. Purified MVM was labeled with Atto-633, while polyclonal human IgGs were bioconjugated with Atto-488 dyes based on chemical crosslinking as previously described [41,47]. Experiments with the fluorescent components were performed on the two morphologically distinct early generation filter membranes Planova 20N and Pegasus SV4.

3.1. Impact of filter fouling in Planova 20N at pH 7.4

Planova 20N represents a commonly used hollow fiber virus filter membrane of the first generation, consisting of regenerated cellulose. The polymer constitutes an asymmetric membrane pore structure with a rough layer at the feed side, followed by a rather shallow pore size gradient, which is conceived to provide high fouling capacity for differently sized fouling species [52–54]. To visualize filter fouling and virus retention within the membrane after VF, the hollow fibers were embedded in agarose and cut orthogonally to obtain circular cross-sections (Fig. 1A) (Supplementary Fig. 1). The filter sections were analyzed by LSM, using the membrane autofluorescence as signal to determine the exact filter dimensions and density profile (Supplementary Fig. 2).

Under defined filtration conditions in PBS only, pH 7.4, and constant flow, the virus retention profile (VRP) shows predominant MVM accumulation in the parvovirus retentive layer at 40–50% of filter depth as previously reported, marking the zone in the membrane where pore sizes are similar to the viral diameter (Fig. 1B and D) [47,48,53,54]. Additionally, a significant number of viruses were retained already within the reservoir zone, where pore sizes are supposed to be predominantly larger than the virus. This early retention is attributed to viruses that are constrained in a minor proportion of retentive voids by the constant convective flow [47]. Expectedly, no significant virus signal was found in the second half of the membrane as this rejection layer, with pores uniformly smaller than the viral diameter, effectively excludes viruses from deeper migration (Fig. 1B and D) [47,48].

To investigate filter membrane fouling mechanisms, we used 1 mg/mL IgG (1% Atto-488 labeled) in PBS, pH 7.4, without stabilizers, as previously described (Fig. 1B and C) [41]. Consequently, a moderate flow decay of 25% after 50L/m^2 was observed, which conforms with precedent reports using comparable feedstream properties (Fig. 1E) [11,41]. Detailed visualization of IgG-488 by LSM showed the expected predominant fouling signal at about 70% of filter depth, corresponding to the smallest pore size of the filter (Fig. 1B and C) [41,53]. These findings further substantiate previous observations suggesting that trace amounts of protein particulates close to the nominal pore size of the membrane represent the main root cause for the decrease in filter performance [11,21,28]. Adsorption of bulk IgG to captured particulates and the membrane polymer further contributes to the flux decline and is influenced by solution pH, conductivity, and stabilizers [18,20,35,55].

In presence of 1 mg/mL IgG, pronounced accumulation of MVM at 45–50% of filter depth was observed, without a shift of the maximal peak depth in comparison to MVM retention in PBS only (Fig. 1B and D). Under these "low-fouling" conditions, however, significantly fewer viruses were observed in the reservoir zone and early retentive layer, where non-retentive pores represent the major proportion, which suggests deeper migration of viral particles in these zones was promoted by the presence of the protein matrix. This phenomenon could be attributed to competition for retentive voids, pore blockage and redirection of the flow to larger pores through foulants, and to flow decay related effects [10,37]. Notably, the migration to a deeper filter depth stands in contrast to previous results using nanoparticles in the same feedstream, where a significant backshift to the feed side was observed [41]. Although VF is predominantly size-dependent, the disparate physico-chemical properties of viruses and artificial nanoparticles may cause differential adsorption and aggregation, which may explain the different retentive behavior [54].

As expected, based on the peak of the VRP remaining at 40–50% depth, virus removal was still effective (LRF >4) with a modest improvement of virus reduction observed at the beginning of filtration (Fig. 1D and F). In summary, under "low-fouling" conditions of 1 mg/mL IgG in PBS, virus retention and capture of the main fouling species does not occur in the same membrane layer; however, an impact of filter fouling on virus retention inside the membrane was already detectable.

To challenge the Planova 20N filter membrane with "high-fouling" conditions, filtration of a feedstream containing 10 mg/mL of polyclonal IgG in PBS, pH 7.4 was performed. An initial rapid flow decay and prolonged filtration at steadily decreasing low flux was observed, similar to profiles describing combined fouling mechanisms during the process (Fig. 1D) [19]. The visualization of the retained IgG within the filter revealed a dramatic shift of the predominant fouling deposition towards the feed side of the filter, showing a remarkably sharp accumulation of the foulants at 25% of filter depth (Fig. 1B and C). This pattern can be interpreted as the formation of an internal cake layer, which was most likely triggered by a combination of distinct mechanisms at higher protein concentrations: i) increased pore constriction/intermediate fouling, thus promoting plugging of pores already in the support layer; ii) presence of larger, self-associated fouling species in the feedstream; iii) increased deposition of bulk protein to retained aggregates as nucleation centers [18,24,29]. The simultaneous occurrence of different fouling mechanisms and dynamic shift of foulant deposition across different membrane zones illustrates the complexity of the VF process in the presence of a protein matrix. Notably, the IgG fouling changed the filter density profile as visualized by the 405 nm measurement, providing an impression regarding the relative amounts of retained IgG under high- and low-fouling conditions (Fig. 1B, Supplementary Fig. 1). The autofluorescence images suggest a markedly increased protein accumulation after filtration of 10 mg/mL IgG feedstream when compared to 1 mg/mL IgG, which is in good agreement with the substantially different flow kinetics observed under these conditions (Fig. 1E).

Analysis of the MVM-633 signal also showed a significant backshift of the VRP towards the feed side (Fig. 1B and D). The shift of filter fouling into the parvovirus retentive layer apparently impacted the retention of the virus, most likely by pore constriction as previously described with nanoparticles [40,41]. However, despite the substantial changes in flow and VRP, LRFs remained at a similar level (Fig. 1F).

The observed retention of both MVM and IgGs in the same filter membrane depth with similar tendencies to backshift under high-fouling conditions suggests that viruses and fouling particulates underlie comparable size-driven mechanisms at these solution properties. However, while the VRP of MVM showed a shift of the retention peak by only 5 μm towards the feed side, the fouling deposition was backshifted by 15–20 μm. This difference can be attributed to the concentration-dependent increase of fouling aggregate size and promoted deposition through adsorption at high protein concentration [18,20].

The 3D scanning of the Planova 20N filter membrane qualitatively confirmed the high-resolution images and quantitative analysis of retention patterns detected in membrane cross-sections, excluding potential artifacts due to the mechanical sectioning, such as distortion of the membrane structure or "smearing" of aggregates across the section surface (Fig. 2A and B). The reconstruction of the stacks demonstrates even retention of fouling particulates and viral particles across a representative area of the Planova 20N membrane, reflecting a uniform filtration and retention process with minimal local variabilities (Fig. 2A). Interestingly, by using MVM as a relevant parvovirus model, we did not observe clusters of retained particles as previously reported with nanoparticles detected in membrane cross-sections [41].

Deposition of fouling species in the filter leads to a physical change of

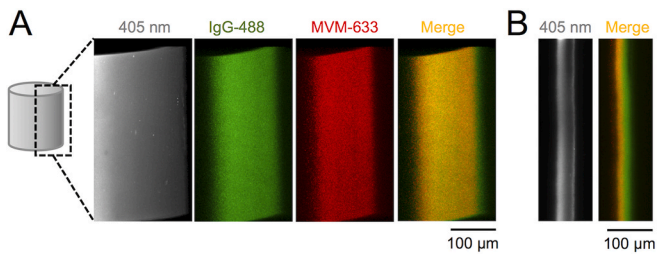

Fig. 2. Laser-scanning microscopy of intact Planova 20N hollow fiber membrane. A) 3D reconstruction of stacked images of Planova 20N hollow fiber after filtration of 10 mg/mL polyclonal human IgG spiked with Atto-488 labeled IgG and Atto-633 labeled MVM (20x objective). B) Cross-section view.

the membrane pore structure, which has a direct effect on virus retention properties. Furthermore, the influence of flux decay needs to be considered as the reduction of the hydrodynamic force increases lateral diffusion and thus the access to non-retentive pathways [37–39,47,56,57]. To distinguish between direct physical effects of filter fouling due to pore constriction, plugging or competition, versus indirect effects due to changes in filter flow, we sought to mimic flow decay in absence of any IgGs by continuously reducing the pressure. Virus retention after flow decay showed a significantly pronounced retention peak at 50% of the filter depth and a minor accumulation in the reservoir zone (Fig. 3A). This VRP stands in sharp contrast to the retention of viruses as broad single peak between 25 and 50% of the filter depth as observed in presence of 10 mg/mL IgG. Therefore, the significant backshift of virus particles from the retentive layer into the support layer under high-fouling conditions can be attributed to the presence of IgG, involving changes in the pore structure such as pore constriction [40,41]. Conversely, the protein in the feedstream appears to also promote deeper migration of viruses particularly in the reservoir zone due to competition for retentive voids, redirection of flow to non-retentive pores, or decreasing adsorptive interactions [10,53].

While LRFs remained above 4 log10 virus removal in filtrations with 10 mg/mL IgG, the artificially induced flow decay led to declined retention capacities (LRFs <4) when operating at low flow as previously reported (Fig. 3C) [39]. Notably, LRFs did not significantly increase at high-fouling conditions despite the remarkable backshift of the VRP, which can be explained by the redirection of the flow to a minor proportion of non-retentive pathways by pore blockage, where viral particles have a high probability to pass through the entire filter membrane [10].

According to the diffusion-based model [38], reduction or absence of the convective flow similarly leads to mobilization of viruses. Interestingly, while both conditions led to a deeper migration and a pronounced retention peak at the rejection layer interface, subtle differences between low flux or flow interruptions were observed in the reservoir zone (Fig. 3A). Repeated pressure releases for 30 min [47] was apparently more effective in mobilizing viruses compared to low flow conditions alone, which might be attributed to the requirement of a completely absent hydrodynamic force or even backflow to escape the larger voids present in this layer [53,57]. In line with this, also the overall retention capacity was more affected by the complete absence of flow, indicating consistent decline of LRFs to 3 log10 virus removal after repeated flow interruptions [47].

Taken together, the detailed visual insights reveal a complex interplay of different, even opposing effects that simultaneously alter virus particle migration or retention in the membrane. In the gradual pore size structure of the Planova 20N membrane, the increased fouling also leads to the formation of alternative selective layers upstream of the original retentive zone. This allows the membrane to compensate for the negative direct and indirect effects such as pore blockage and flow decay.

3.2. Impact of filter fouling in Pegasus SV4 at pH 7.4

The Pegasus SV4 filter is composed of two identical flat-sheet membranes and can be considered as an intermediate representative between the first and second filter generation. This filter has often been referred as a symmetric membrane type; however, structural, and functional analyses of the filter illustrate the presence of a thin support layer of a few micrometers at the feed side of both membrane layers [46,58]. The two membranes each comprise a thick homogenous layer with pore sizes predominantly smaller than the virus diameter. Filtration performed in PBS only and normal flow resulted in the known MVM retention at the beginning of the first filter membrane [46,47], and viruses were effectively removed during normal flow filtration conditions (LRF >5) (Fig. 4A, D and F).

Addition of 1 mg/mL IgG to the feedstream and visualization of the co-spiked IgG-488 revealed a predominant retention of IgG within 0–30% filter depth of the first membrane and a strongly reduced signal in the same region of the second membrane (Fig. A and C). The asymmetric retention of the fouling species by the first membrane similar to a prefilter correlates with a size-exclusion mechanism, demonstrating that the major fouling by this feedstream involves protein aggregates [18,43]. This fouling decreased the flux by 40% after 50L/m^2 when compared to PBS only conditions (Fig. 4E). Similar to buffer conditions, MVM retention was found in the first micrometers without any significant breakthrough to the second membrane layer (Fig. 4A and D). Although virus retention and filter fouling apparently occur in the same region of this filter, no visible negative or positive impact on virus retention under these "low-fouling" conditions was detected. In line with this, overall virus retention remained consistent, indicating robust removal of viruses from the filtrate (Fig. 4F).

Significant flow decay was observed when challenging the Pegasus SV4 filter with 10 mg/mL IgG, mirroring results achieved with the Planova 20N filter (Figs. 1 and 4E). However, in contrast to the backshift of retained foulants towards the feed side in the Planova 20N, fouling

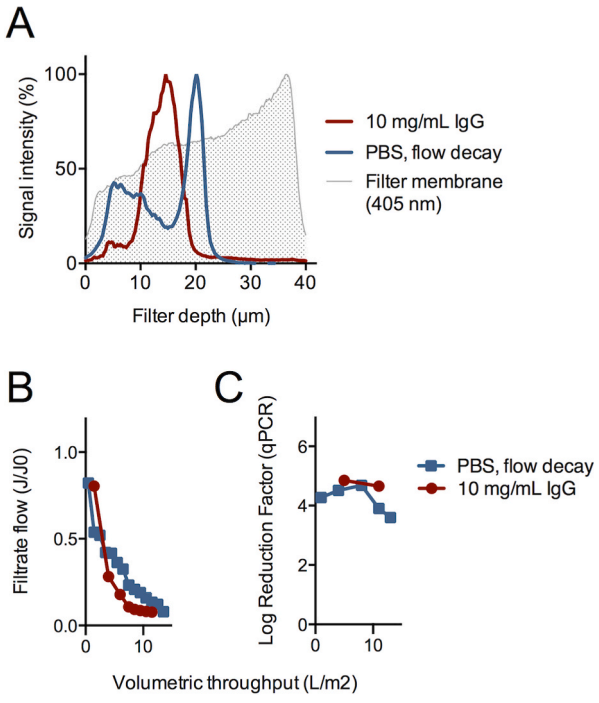

Fig. 3. Effect of flow decay on parvovirus retention in Planova 20N membrane. A) Comparison of MVM retention profiles in the filter membrane after gradual reduction of pressure (PBS, flow decay) to mimic fouling-induced flow decay obtained after filtration of 10 mg/mL IgG in PBS. B) Detected flow decay as consequence of gradual pressure reduction or fouling by 10 mg/mL IgG. C) Log10 reduction factors (LRFs) of MVM in filtrate fractions as determined by qPCR. Graphs show one filtration per condition (n = 1).

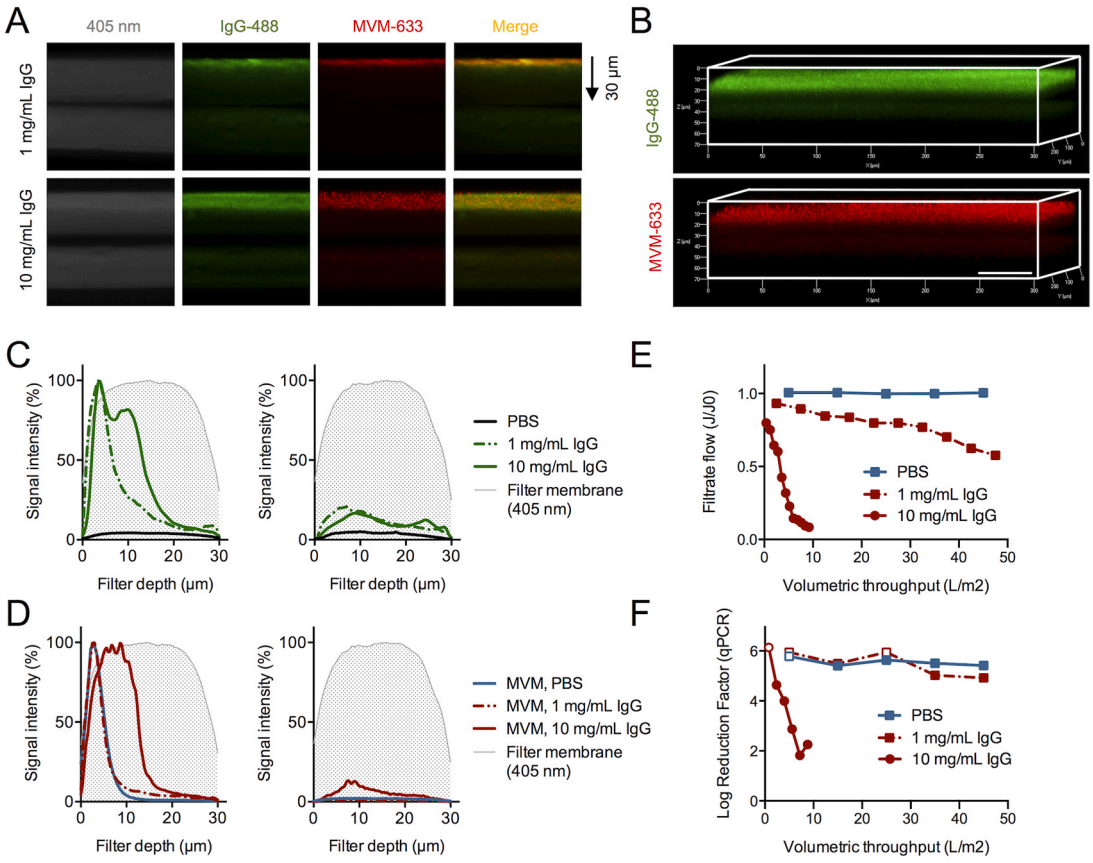

Fig. 4. Filter fouling and parvovirus retention in Pegasus SV4 double layer membrane. A) Laser-scanning microscopy images of Pegasus SV4 double membrane cross-section after filtration of 1 mg/mL or 10 mg/mL IgG spiked with Atto-488 labeled IgG in a proportion of 1:100 and Atto-633 labeled MVM (63x objective). B) 3D analysis of intact double layer membrane segments after filtration of 10 mg/mL IgG (20x objective). Retention profiles of C) IgG foulants and D) MVM-633 in the first (left panels) and second (right panels) membrane layer based on ImageJ analysis [50]. E) Relative filter flow (J/J0) of different feedstreams. F) Log10 reduction factors (LRFs) determined by qPCR of virions in feed and filtrate samples. Graphs show one filtration per condition (n = 1).

species penetrated deeper into the Pegasus SV4 filter (Fig. 4A–C) (Supplementary Fig. 3). The abrupt decline of signal at 50% filter depth of the first membrane layer and the significant passage of fouling species directly to the second filter membrane suggests that at filter depth 50–100% the Pegasus SV4 membranes do not provide any additional foulant capture properties. Assuming a predominantly size-based accumulation of fouling species, this implies that smallest pore sizes are found at approximately 50% depth of the Pegasus SV4 filter membranes. This forward shift of foulants into the filter at high-fouling conditions could be attributed to competition among fouling particulates for retentive pores, redirection of the flow to larger pores, and increasing diffusion due to flow decay [10]. The retained aggregates likely serve as nucleation sites for additional adsorption of bulk protein, forming a layer of foulants at the beginning of the first membrane that expands into the filter with increasing throughput [18,24].

Further differences in the fouling mechanisms between the Pegasus SV4 and Planova 20N filter became evident when comparing the impact on parvovirus retention. In the Pegasus SV4, MVM was found to migrate significantly deeper into the first membrane layer under high-fouling conditions (Fig. 4A and D) (Supplementary Fig. 3). Similar to the retained fouling IgG species, the signal abruptly decreased at about 40–50% of filter depth, indicating a significant proportion of viral particles passed to the second membrane layer. This significant penetration of the Pegasus SV4 filter membrane corroborates previous findings that this membrane type does not provide a strict rejection layer of uniform pore sizes that would exclude deeper migration of viruses under challenging conditions [23,47,59].

Scanning of an intact Pegasus SV4 double layer membrane segment in 3D mode showed a uniform retention of viruses and fouling particulates as well as an evenly distributed passage of both entities to the second membrane layer (Fig. 4B) (Supplementary Fig. 3B). In accordance with the observed forward shift of the VRP peak in flow direction, virus removal capacities were substantially decreased (LRF = 2) when operating under high-fouling conditions, which is in line with previous reports (Fig. 4F) [12,60].

To dissect the impact of direct fouling mechanisms from effects related to flux decline, we again mimicked flow decay by stepwise reduction of the pressure in absence of IgGs. Remarkably, the artificial flow decay did not cause the deep migration of viral particles as observed in the presence of 10 mg/mL IgG (Fig. 5A). This demonstrates that the physical presence of foulants in the feedstream directly promotes the penetration of viruses into deeper layers of the Pegasus SV4 membrane, possibly through pore competition and redirection of the flow to larger pores [10]. Under artificial flow decay, LRFs decreased in a delayed manner when compared to fouling-induced flux decline (Fig. 5B and C). This observation conforms with the diffusion-based model that the hydrodynamic force of the convective flow constrains virus particles in retentive voids until reaching a certain low-flow threshold with the subsequent breakthrough occurring in a time-dependent manner [12,56,57].

Taken together, these results reveal significantly different fouling mechanisms, as well as distinct impacts of fouling and flow rate on virus particle retention, depending on the membrane type. In asymmetric membranes with a defined pore size gradient, fouling through adsorption to the membrane can result in a gradual pore constriction across different membrane zones (Fig. 6). The shift of the pore size gradient

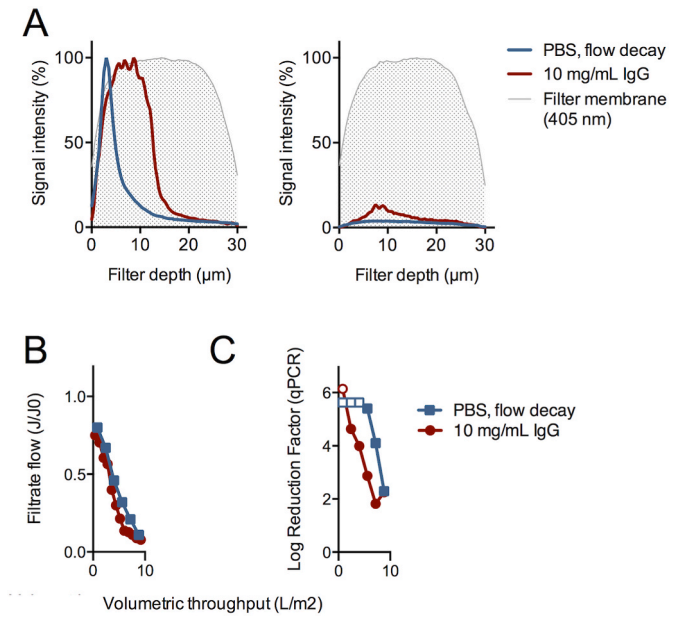

Fig. 5. Effect of flow decay on parvovirus retention in Pegasus SV4 filter. A) Comparison of MVM retention profiles in filter membrane layers after gradual reduction of pressure (PBS, flow decay) to mimic fouling-induced flow decay obtained during filtration of 10 mg/mL IgG in PBS. B) Detected flow decay as consequence of gradual pressure reduction or fouling by 10 mg/mL IgG. C) Log10 reduction factors (LRFs) of MVM determined by qPCR. Graphs show one filtration per condition (n = 1).

towards the feed side, which apparently correlates with the degree of fouling, generates alternative selective layers upstream of the original parvovirus retentive zone with the capability to effectively retain the virus. Homogenous membranes with a fairly symmetric structure, however, only have a thin support layer upstream of the functional layer that can provide gradual capture of foulants and particles, thus protecting the actual retentive zone. (Fig. 6). Therefore, the capacity for beneficial pore constriction effects is limited in this membrane morphology and is more susceptible to feedstreams with high-fouling properties.

Albeit negative fouling effects that promote deeper migration of particles were visually detectable in both filter types, they were more dominant in the nearly homogeneous filter structure when operating at high-fouling conditions. The membrane morphology of the Pegasus SV4, which lacks a strict rejection layer, provided effective virus retention under limited fouling and normal flow conditions; however, beyond a certain limit of fouling and low-pressure, negative effects appeared to combine synergistically, promoting deeper migration of filtered particulates in the retentive layer, resulting in a drastic decrease of the virus retention capacity (Figs. 5C and 6). In contrast, fouling-related deeper migration of MVM in the asymmetric Planova 20N was mainly apparent in the reservoir zone, while being less pronounced or compensated by pore constriction in the retentive layer.

Finally, the comparison of VRPs analyzed after similar or different volumetric throughputs (Figs. 1D, 3A and 4D, Fig. 5A) [47] consistently demonstrated that differences in the retention of the viruses were associated to the tested fouling or flow conditions but not a consequence of variations in the total viral load.

The preceding results were generated by using "standard" conditions of IgG in PBS, pH 7.4, to facilitate the comparison to previous studies [40,41]. However, from the perspective of process performance, these "artificial" conditions are known to be suboptimal for polyclonal IgGs, as the pH conditions overlap with the pI range of these molecules (pI 6.5–9), which accordingly promotes intra- and intermolecular hydrophobic interactions and the formation of fouling particulates [11,33].

3.3. *Impact of filter fouling under manufacturing-like conditions*

Conditions for manufacturing polyclonal human IgGs are selected to minimize self-association and irreversible hydrophobic interactions of the therapeutic product. Accordingly, VF is commonly carried out in the range of pH 4.5–5.5 to operate significantly below the IgGs pI. Highly pure IgG product intermediates and optimized conditions are essential as even minor portions of subvisual particulates in the feedstream can substantially limit virus filter performance [11,20,28]. Generally, protein concentrations of 5–20 mg/mL represent a reasonable compromise between throughput, flow, and fouling [29,35].

To investigate filter performance and virus retention in context of real manufacturing conditions, we conducted filtrations with a relevant IgG product intermediate (phosphate-acetate buffer, pH 4.8, ~10–14 mg/mL IgG, 0.5 mS/cm). In both filters tested, the flux was similarly reduced to J/J0 = 0.5 and remained constant over the filtration process (Fig. 7A). The absence of significant flow decay demonstrates minimal irreversible fouling by this feedstream, while the reduction of flow can be mainly attributed to reversible fouling through electrostatic interactions and solution viscosity [29,35].

Fouling of this IgG product intermediate could not be visualized by the Atto-488 bioconjugation considering the commonly used labeling approach is not compatible with the pH and buffer species of this solution. Nevertheless, the autofluorescence profile at 405 nm indicated no significant accumulation of foulants at a particular filter depth in both filters, which underlines the absence of detectable protein aggregates in this purified biotherapeutic product (Supplementary Fig. 4).

Visualization of MVM within both filter membranes revealed a tendency for an earlier retention of the virus compared to PBS only, suggesting an increased stringency in size-based sieving caused by pore constriction under these manufacturing-like conditions (Fig. 7C and D).

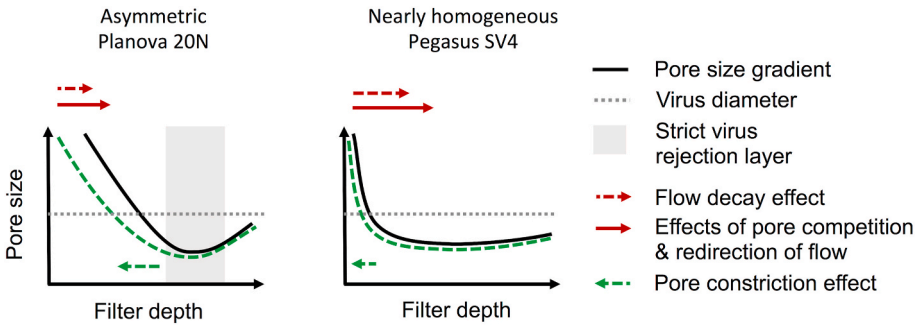

Fig. 6. Schematic depiction of observed fouling effects on virus retention in distinct membrane morphologies. Solid line indicates expected pore size gradient of pristine Planova 20N and Pegasus SV4 membranes as based on current results and previous reports [46,47,53,54,58]. The strict rejection layer constitutes pore sizes uniformly smaller than the parvovirus diameter (MVM), which excludes deeper migration of viruses also under challenging conditions [47]. Dashed green line illustrates suggested pore size gradient as a consequence of fouling-related pore constriction, leading to backshifted particle retention. Red arrows combine for direct fouling effects as pore competition, pore blockage, redirection of flow to larger pores, as well as indirect impact of flow decay, which together promote deeper migration of particulates. (For interpretation of the references to colour in this figure legend, the reader is referred to the Web version of this article.)

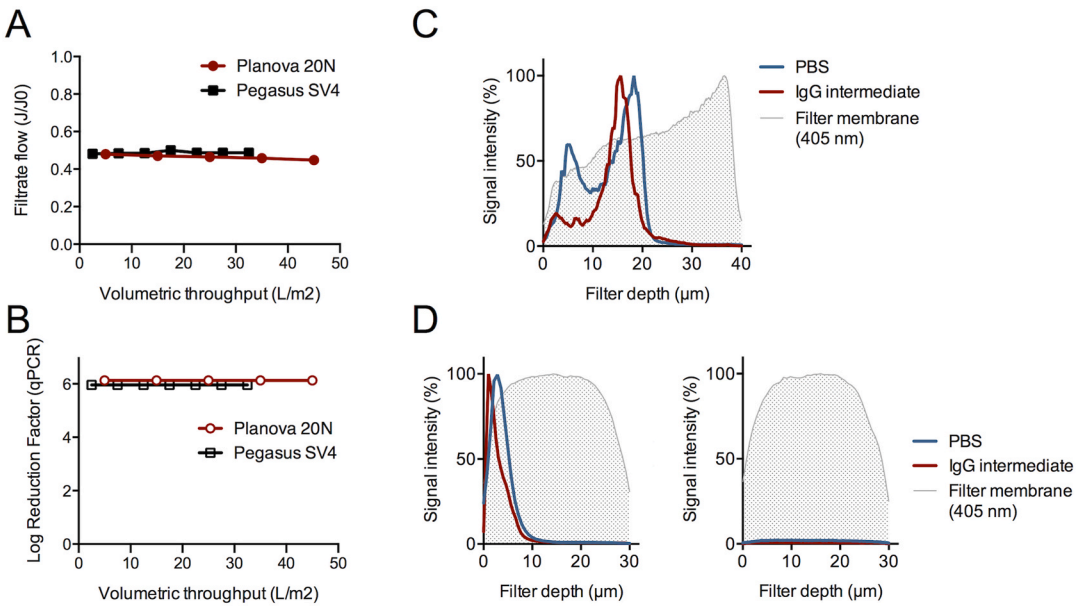

Fig. 7. Virus filtration of a relevant IgG product intermediate in Planova 20N and Pegasus SV4 filters. A) Detected flux during filtration of a IgG product intermediate representing a relevant feedstream in manufacturing. B) Log10 reduction factors (LRFs) of MVM determined by qPCR. MVM retention profiles in (C) Planova 20N and (D) Pegasus SV4 filter membranes after filtration of a IgG product intermediate in comparison to PBS. Graphs show one filtration per condition (n = 1).

In fact, increased adsorption of IgG to the membrane through electrostatic interaction can be anticipated based on the measured zeta-potentials at this pH [35,39]. Interestingly, mobilization effects and deeper migration of MVM in the reservoir zone of the Planova 20N were still evident in comparison to the minor peak observed in PBS only, implying remaining opposing effects by the product on virus capture within the membrane. Besides the size-based fouling mechanisms, additional effects due to adsorptive interactions between the virus, the membrane, and the therapeutic protein may further contribute to an altered virus retention under these conditions. In agreement with the backshift of virus retention towards the feed side, virus removal in both filters was found to be more effective in this product feedstream, indicating no detectable virions in the filtrate fractions (Fig. 7B).

In summary, the performance of both filters improved significantly under manufacturing-like conditions of a relatively pure IgG product intermediate when compared to results using a research-grade polyclonal IgG sample in PBS, pH 7.4. These findings exemplify that care should be taken when drawing conclusions from basic research studies on membrane fouling to relevant manufacturing conditions. Nevertheless, both approaches are needed to obtain a complete picture of the process, a deep understanding of the individual factors at defined "standard" conditions, as well as the visualization of the virus in a representative, but complex product feedstream.

4. Conclusion

The objective of this work was to gain mechanistic insights into protein fouling and its effect on virus retention by using the relevant parvovirus model MVM, which is commonly used in validation studies performed in biopharmaceutical industry settings. The visualization of IgG fouling species within two distinct virus filter membranes revealed the occurrence of characteristic fouling phenomena, such as gradual pore constriction and internal cake formation, which strongly depended on the membrane morphologies and conditions. Dissecting the effect of flow decay and fouling demonstrated a significant impact on the virus retention due to the presence of protein foulants, illustrating a transition to a membrane pore structure with altered virus selective properties. While both tested filter membranes showed effective virus retention under low-fouling or manufacturing-like conditions, fundamental differences in virus clearance performance were found when challenged with a high-fouling feedstream. The results suggest a complex interplay of different fouling phenomena with synergistic or opposing effects on particle retention. Future studies are warranted to better dissect the impact of these factors and thus to gain further insights into the underlying mechanisms. A better understanding of the process will help to optimize the performance and virus retention capacity of virus filter membranes, facilitating a cost-effective downstream process and high safety of biotherapeutic products.

CRediT authorship contribution statement

Remo Leisi: Conceptualization, Methodology, Investigation, Formal analysis, Writing - original draft, Writing - review & editing. Iman Rostami: Investigation, Formal analysis. Andrew Laughhunn: Conceptualization, Funding acquisition, Writing - review & editing. Jan Bieri: Investigation, Writing - review & editing. Nathan J. Roth: Conceptualization, Funding acquisition, Writing - review & editing. Eleonora Widmer: Conceptualization, Funding acquisition, Writing - review & editing, Supervision. Carlos Ros: Conceptualization, Writing - original draft, Writing - review & editing, Supervision, Project administration.

Declaration of competing interest

The authors declare the following financial interests/personal relationships which may be considered as potential competing interests: Remo Leisi, Andrew Laughhunn, Eleonora Widmer, and Nathan J. Roth are employees of CSL Behring, a biotechnology company, which uses virus filters in its manufacturing. The authors declare no conflicts of interest

Data availability

Data will be made available on request.

Acknowledgments

We would like to acknowledge the University of Bern and CSL Behring AG for their support of this work.

Appendix A. Supplementary data

Supplementary data to this article can be found online at https://doi.org/10.1016/j.memsci.2022.120791.

References

[1] M.M. Lieber, R.E. Benveniste, D.M. Livingston, G.J. Todaro, Mammalian cells in culture frequently release type C viruses, Science 182 (1973) 56–58, https://doi.org/10.1126/science.182.4107.56 (80-.).

[2] P.W. Barone, M.E. Wiebe, J.C. Leung, I.T.M. Hussein, F.J. Keumurian, J. Bouressa, A. Brussel, D. Chen, M. Chong, H. Dehghani, L. Gerentes, J. Gilbert, D. Gold, R. Kiss, T.R. Kreil, R. Labatut, Y. Li, J. Müllberg, L. Mallet, C. Menzel, M. Moody, S. Monpoeho, M. Murphy, M. Plavsic, N.J. Roth, D. Roush, M. Ruffing, R. Schicho, R. Snyder, D. Stark, C. Zhang, J. Wolfrum, A.J. Sinskey, S.L. Springs, Viral contamination in biologic manufacture and implications for emerging therapies, Nat. Biotechnol. (2020), https://doi.org/10.1038/s41587-020-0507-2.

[3] I.C.H. Q5A Guideline, Viral Safety Evaluation Of Biotechnology Products Derived From Cell Lines Of Human Or Animal Origin, 1999.

[4] M. Moody, W. Alves, J. Varghese, F. Khan, Mouse minute virus (MMV) contamination - a case study: detection, root cause determination, and corrective actions, PDA J. Pharm. Sci. Technol. (2011) 580–588, https://doi.org/10.5731/pdajpst.2011.00824.

[5] E. Gefroh, H. Dehghani, M. McClure, L. Connell-Crowley, G. Vedantham, Use of MMV as a single worst-case model virus in viral filter validation studies, PDA J. Pharm. Sci. Technol. 68 (2014) 297–311, https://doi.org/10.5731/pdajpst.2014.00978.

[6] N.J. Roth, H.O. Dichtelmüller, F. Fabbrizzi, E. Flechsig, A. Gröner, M. Gustafson, J. I. Jorquera, T.R. Kreil, D. Misztela, E. Moretti, M. Moscardini, G. Poelsler, J. More, P. Roberts, A. Wieser, R. Gajardo, Nanofiltration as a robust method contributing to viral safety of plasma-derived therapeutics: 20 years' experience of the plasma protein manufacturers, Transfusion 60 (2020) 2661–2674, https://doi.org/10.1111/trf.16022.

[7] A.L. Llamas-Saiz, M. Agbandje-McKenna, W.R. Wikoff, J. Bratton, P. Tattersall, M. G. Rossmann, Structure determination of minute virus of mice, Acta Crystallogr. Sect. D Biol. Crystallogr. 53 (1997) 93–102, https://doi.org/10.1107/S0907444996010566.

[8] B. Kaufmann, A.A. Simpson, M.G. Rossmann, The structure of human parvovirus B19, Proc. Natl. Acad. Sci. U. S. A 101 (2004) 11628–11633, https://doi.org/10.1073/pnas.0402992101.

[9] V.S. Reddy, P. Natarajan, B. Okerberg, K. Li, K.V. Damodaran, R.T. Morton, C. L. Brooks, J.E. Johnson, Virus particle explorer (VIPER), a website for virus capsid structures and their computational analyses, J. Virol. 75 (2001) 11943–11947, https://doi.org/10.1128/jvi.75.24.11943-11947.2001.

[10] G. Bolton, M. Cabatingan, M. Rubino, S. Lute, K. Brorson, M. Bailey, Normal-flow virus filtration: detection and assessment of the endpoint in bioprocessing, Biotechnol. Appl. Biochem. 42 (2005) 133, https://doi.org/10.1042/ba20050056.

[11] W.J. Rayfield, D.J. Roush, R.A. Chmielowski, N. Tugcu, S. Barakat, J.K. Cheung, Prediction of viral filtration performance of monoclonal antibodies based on biophysical properties of feed, Biotechnol. Prog. 31 (2015) 765–774, https://doi.org/10.1002/btpr.2094.

[12] L. David, J. Niklas, B. Budde, M. Lobedann, G. Schembecker, Continuous viral filtration for the production of monoclonal antibodies, Chem. Eng. Res. Des. 152 (2019) 336–347, https://doi.org/10.1016/j.cherd.2019.09.040.

[13] J. Hermia, Constant pressure blocking filtration laws - application TOPOWER-law NON-Newtonian fluids, Trans. Inst. Chem. Eng. 60 (1982) 183–187.

[14] G. Belfort, R.H. Davis, A.L. Zydney, The behavior of suspensions and macromolecular solutions in crossflow microfiltration, J. Membr. Sci. (1994), https://doi.org/10.1016/0376-7388(94)00119-7.

[15] C.C. Ho, A.L. Zydney, A combined pore blockage and cake filtration model for protein fouling during microfiltration, J. Colloid Interface Sci. 232 (2000) 389–399, https://doi.org/10.1006/jcis.2000.7231.

[16] G.R. Bolton, A.W. Boesch, M.J. Lazzara, The effects of flow rate on membrane capacity: development and application of adsorptive membrane fouling models, J. Membr. Sci. 279 (2006) 625–634, https://doi.org/10.1016/j.memsci.2005.12.057.

[17] G. Bolton, D. LaCasse, R. Kuriyel, Combined models of membrane fouling: development and application to microfiltration and ultrafiltration of biological fluids, J. Membr. Sci. 277 (2006) 75–84, https://doi.org/10.1016/j.memsci.2004.12.053.

[18] D.M. Kanani, X. Sun, R. Ghosh, Reversible and irreversible membrane fouling during in-line microfiltration of concentrated protein solutions, J. Membr. Sci. 315 (2008) 1–10, https://doi.org/10.1016/j.memsci.2008.01.053.

[19] F.N.U. Namila, D. Zhang, S. Traylor, T. Nguyen, N. Singh, R. Wickramasinghe, X. Qian, The effects of buffer condition on the fouling behavior of MVM virus filtration of an Fc-fusion protein, Biotechnol. Bioeng. 116 (2019) 2621–2631, https://doi.org/10.1002/bit.27085.

[20] S.T. Kelly, W. Senyo Opong, A.L. Zydney, The influence of protein aggregates on the fouling of microfiltration membranes during stirred cell filtration, J. Membr. Sci. 80 (1993) 175–187, https://doi.org/10.1016/0376-7388(93)85142-J.

[21] Z.H. Syedain, D.M. Bohonak, A.L. Zydney, Protein fouling of virus filtration membranes: effects of membrane orientation and operating conditions, Biotechnol. Prog. 22 (2006) 1163–1169, https://doi.org/10.1021/bp050350v.

[22] G.R. Bolton, J. Basha, D.P. LaCasse, Achieving high mass-throughput of therapeutic proteins through parvovirus retentive filters, Biotechnol. Prog. 26 (2010) 1671–1677, https://doi.org/10.1002/btpr.494.

[23] P. Kosiol, C. Kahrs, V. Thom, M. Ulbricht, B. Hansmann, Investigation of virus retention by size exclusion membranes under different flow regimes, Biotechnol. Prog. 35 (2019), https://doi.org/10.1002/btpr.2747.

[24] S.T. Kelly, A.L. Zydney, Effects of intermolecular thiol–disulfide interchange reactions on bsa fouling during microfiltration, Biotechnol. Bioeng. 44 (1994) 972–982, https://doi.org/10.1002/bit.260440814.

[25] M. Bakhshayeshi, A.L. Zydney, Effect of solution pH on protein transmission and membrane capacity during virus filtration, Biotechnol. Bioeng. 100 (2008) 108–117, https://doi.org/10.1002/bit.21735.

[26] F. Fallahianbijan, P. Emami, J.M. Hillsley, S.P. Motevalian, B.C. Conde, K. Reilly, A.L. Zydney, Effect of membrane pore structure on fouling behavior of glycoconjugate vaccines, J. Membr. Sci. 619 (2021), https://doi.org/10.1016/j.memsci.2020.118797.

[27] G.R. Bolton, S. Spector, D. LaCasse, Increasing the capacity of parvovirus-retentive membranes: performance of the Viresolve™ Prefilter, Biotechnol. Appl. Biochem. 43 (2006) 55, https://doi.org/10.1042/ba20050108.

[28] A. Brown, C. Bechtel, J. Bill, H. Liu, J. Liu, D. McDonald, S. Pai, A. Radhamohan, R. Renslow, B. Thayer, S. Yohe, C. Dowd, Increasing parvovirus filter throughput of monoclonal antibodies using ion exchange membrane adsorptive pre-filtration, Biotechnol. Bioeng. 106 (2010) 627–637, https://doi.org/10.1002/bit.22729.

[29] E.M. Goodrich, D.M. Bohonak, P.W. Genest, E. Peterson, Recent advances in ultrafiltration and virus filtration for production of antibodies and related biotherapeutics, in: Approaches to Purification, Anal. Charact. Antibody-Based Ther., 2020, pp. 137–166, https://doi.org/10.1016/b978-0-08-103019-6.00007-2.

[30] A. Tang, I. Ramos, K. Newell, K.D. Stewart, A novel high-throughput process development screening tool for virus filtration, J. Membr. Sci. 611 (2020), https://doi.org/10.1016/j.memsci.2020.118330.

[31] V. Stanevich, A. Pachalla, B. Nunez, M. McInnes, C. Nieder, J. Schreffler, Improving viral filtration capacity in biomanufacturing processes using aggregate binding properties of polyamide-6,6, Biotechnol. Bioeng. 118 (2021) 1105–1115, https://doi.org/10.1002/bit.27634.

[32] A.G. Fane, C.J.D. Fell, A. Suki, The effect of ph and ionic environment on the ultrafiltration of protein solutions with retentive membranes, J. Membr. Sci. 16 (1983) 195–210, https://doi.org/10.1016/S0376-7388(00)81310-1.

[33] S.P. Palecek, A.L. Zydney, Hydraulic permeability of protein deposits formed during microfiltration: effect of solution pH and ionic strength, J. Membr. Sci. 95 (1994) 71–81, https://doi.org/10.1016/0376-7388(94)85030-5.

[34] Y.P. Lim, A.W. Mohammad, Effect of solution chemistry on flux decline during high concentration protein ultrafiltration through a hydrophilic membrane, Chem. Eng. J. 159 (2010) 91–97, https://doi.org/10.1016/j.cej.2010.02.044.

[35] T. Hongo-Hirasaki, M. Komuro, S. Ide, Effect of antibody solution conditions on filter performance for virus removal filter PlanovaTM 20N, Biotechnol. Prog. 26 (2010) 1080–1087, https://doi.org/10.1002/btpr.415.

[36] S. Lute, M. Bailey, J. Combs, M. Sukumar, K. Brorson, Phage passage after extended processing in small-virus-retentive filters, Biotechnol. Appl. Biochem. 47 (2007) 141, https://doi.org/10.1042/ba20060254.

[37] R. Fan, F. Namila, D. Sansongko, S.R. Wickramasinghe, M. Jin, D. Kanani, X. Qian, The effects of flux on the clearance of minute virus of mice during constant flux virus filtration, Biotechnol. Bioeng. 118 (2021) 3511–3521, https://doi.org/10.1002/bit.27778.

[38] A. Yamamoto, T. Hongo-Hirasaki, Y. Uchi, H. Hayashida, F. Nagoya, Effect of hydrodynamic forces on virus removal capability of Planova™ filters, AIChE J. 60 (2014) 2286–2297, https://doi.org/10.1002/aic.14392.

[39] D. Strauss, J. Goldstein, T. Hongo-Hirasaki, Y. Yokoyama, N. Hirotomi, T. Miyabayashi, D. Vacante, Characterizing the impact of pressure on virus filtration processes and establishing design spaces to ensure effective parvovirus removal, Biotechnol. Prog. 33 (2017) 1294–1302, https://doi.org/10.1002/btpr.2506.

[40] F. Fallahianbijan, S. Giglia, C. Carbrello, D. Bell, A.L. Zydney, Impact of protein fouling on nanoparticle capture within the Viresolve® Pro and Viresolve® NFP virus removal membranes, Biotechnol. Bioeng. 116 (2019) 2285–2291, https://doi.org/10.1002/bit.27017.

[41] H. Nazem-Bokaee, D. Chen, S.M. O'Donnell, A.L. Zydney, Visualizing effects of protein fouling on capture profiles in the Planova BioEX and 20N virus filters, J. Membr. Sci. 610 (2020), https://doi.org/10.1016/j.memsci.2020.118271.

[42] S.K. Dishari, M.R. Micklin, K.J. Sung, A.L. Zydney, A. Venkiteshwaran, J.N. Earley, Effects of solution conditions on virus retention by the Viresolve® NFP filter, Biotechnol. Prog. 31 (2015) 1280–1286, https://doi.org/10.1002/btpr.2125.

[43] P. Emami, F. Fallahianbijan, E. Dinse, S.P. Motevalian, B.C. Conde, K. Reilly, A. L. Zydney, Modified intermediate pore blockage model describes fouling behavior during sterile filtration of glycoconjugate vaccines, J. Membr. Sci. 613 (2020), https://doi.org/10.1016/j.memsci.2020.118495.

[44] C.S. Widing, N.R. Ruffle-Deignan, E.M.S. Stennett, Imaging and identifying BSA biofouling through the combination of fluorescence microscopy and flux experiments, Clean - soil, Air, Water 49 (2021), https://doi.org/10.1002/clen.202000326.

[45] R. Leisi, R. Wolfisberg, T. Nowak, O. Caliaro, A. Hemmerle, N.J. Roth, C. Ros, Impact of the isoelectric point of model parvoviruses on viral retention in anion-exchange chromatography, Biotechnol. Bioeng. 118 (2021) 116–129, https://doi.org/10.1002/bit.27555.

[46] R. Leisi, J. Bieri, N.J. Roth, C. Ros, Determination of parvovirus retention profiles in virus filter membranes using laser scanning microscopy, J. Membr. Sci. 603 (2020), https://doi.org/10.1016/j.memsci.2020.118012.

[47] R. Leisi, E. Widmer, B. Gooch, N.J. Roth, C. Ros, Mechanistic insights into flow-dependent virus retention in different nanofilter membranes, J. Membr. Sci. 636 (2021), https://doi.org/10.1016/j.memsci.2021.119548.
[48] T. Hongo-Hirasaki, K. Yamaguchi, K. Yanagida, H. Hayashida, S. Ide, Effects of varying virus-spiking conditions on a virus-removal filter Planova^{TM} 20N in a virus validation study of antibody solutions, Biotechnol. Prog. 27 (2011) 162–169, https://doi.org/10.1002/btpr.533.
[49] D. Cetlin, M. Pallansch, C. Fulton, E. Vyas, A. Shah, T. Sohka, A. Dhar, L. Pallansch, D. Strauss, Use of a noninfectious surrogate to predict minute virus of mice removal during nanofiltration, Biotechnol. Prog. 34 (2018) 1213–1220, https://doi.org/10.1002/btpr.2694.
[50] C.A. Schneider, W.S. Rasband, K.W. Eliceiri, NIH Image to ImageJ: 25 years of image analysis, Nat. Methods (2012), https://doi.org/10.1038/nmeth.2089.
[51] S. Ideno, K. Takahashi, K. Yusa, K. Sakai, Quantitative PCR evaluation of parvovirus B19 removal via nanofiltration, J. Virol. Methods. 275 (2020), https://doi.org/10.1016/j.jviromet.2019.113755.
[52] B.F. Marques, D.J. Roush, K.E. Göklen, Virus filtration of high-concentration monoclonal antibody solutions, Biotechnol. Prog. 25 (2009) 483–491, https://doi.org/10.1002/btpr.177.
[53] J. Adan-Kubo, M. Tsujikawa, K. Takahashi, T. Hongo-Hirasaki, K. Sakai, Microscopic visualization of virus removal by dedicated filters used in biopharmaceutical processing: impact of membrane structure and localization of captured virus particles, Biotechnol. Prog. 35 (2019), https://doi.org/10.1002/btpr.2875.
[54] P. Kosiol, M.T. Müller, B. Schneider, B. Hansmann, V. Thom, M. Ulbricht, Determination of pore size gradients of virus filtration membranes using gold nanoparticles and their relation to fouling with protein containing feed streams, J. Membr. Sci. 548 (2018) 598–608, https://doi.org/10.1016/j.memsci.2017.11.048.
[55] R. Hamamoto, H. Ito, M. Hirohara, R. Chang, T. Hongo-Hirasaki, T. Hayashi, Interactions between protein molecules and the virus removal membrane surface: effects of immunoglobulin G adsorption and conformational changes on filter performance, Biotechnol. Prog. 34 (2018) 379–386, https://doi.org/10.1002/btpr.2586.
[56] D. LaCasse, S. Lute, M. Fiadeiro, J. Basha, M. Stork, K. Brorson, R. Godavarti, C. Gallo, Mechanistic failure mode investigation and resolution of parvovirus retentive filters, Biotechnol. Prog. 32 (2016) 959–970, https://doi.org/10.1002/btpr.2298.
[57] H. Wu, Y. Cai, D.K. Schwartz, Particle remobilization in filtration membranes during flow interruption, J. Membr. Sci. 610 (2020), https://doi.org/10.1016/j.memsci.2020.118405.
[58] M. Billups, M. Minervini, M. Holstein, H. Feroz, S. Ranjan, J. Hung, H. Bao, S. Ghose, Z.J. Li, A.L. Zydney, Antibody retention by virus filtration membranes: polarization and sieving effects, J. Membr. Sci. 620 (2021), https://doi.org/10.1016/j.memsci.2020.118884.
[59] P. Kosiol, B. Hansmann, M. Ulbricht, V. Thom, Determination of pore size distributions of virus filtration membranes using gold nanoparticles and their correlation with virus retention, J. Membr. Sci. 533 (2017) 289–301, https://doi.org/10.1016/j.memsci.2017.03.043.
[60] T. Nowak, B. Popp, N.J. Roth, Choice of parvovirus model for validation studies influences the interpretation of the effectiveness of a virus filtration step, Biologicals 60 (2019) 85–92, https://doi.org/10.1016/j.biologicals.2019.04.003.